THE ASTROPHYSICAL JOURNAL, 403:517–529, 1993 February 1

THE INFLUENCE OF CORE RADIUS ON GRAVITATIONAL LENSING BY ELLIPTICAL LENSES

SYLVANIE WALLINGTON AND RAMESH NARAYAN
Harvard-Smithsonian Center for Astrophysics, 60 Garden Street, Cambridge, MA 02138
Received 1992 April 9; accepted 1992 August 5

ABSTRACT

We model a galaxy lens by means of a simple analytical potential with three parameters: velocity dispersion, ellipticity, and core radius. We compute lensing cross sections for a wide range of these parameters and integrate over the distributions of velocity dispersion and ellipticity appropriate to galaxies. The model predictions are in good agreement with the observations. The number of lensed quasars as a function of apparent magnitude and the relative numbers of doubly imaged and quadruply imaged quasars are predicted satisfactorily. Magnification bias is found to be extremely large at bright magnitudes, particularly for quadruply imaged configurations. The presence of an even number of images in nearly all examples of multiply imaged quasars discovered so far, despite the odd number expected theoretically, can be explained through demagnification of an image in the core of the lens. This requires lens core radii to be smaller than about 200 pc.

Subject headings: galaxies: fundamental parameters — gravitational lensing — quasars: general

1. INTRODUCTION

In the dozen years since the "double quasar" Q0957+561 was discovered (Walsh, Carswell, & Weymann 1979), gravitational lensing has become an active branch of extragalactic astronomy (for reviews see Blandford & Kochanek 1987a; Surdej 1990; Fort 1992; Blandford & Narayan 1992; Schneider, Ehlers, & Falco 1992). Many kinds of lensing phenomena have been discovered and studied, e.g., multiply imaged quasars, luminous arcs, and radio rings.

This paper is concerned with multiply imaged quasars. In these sources, a high-redshift quasar happens to lie behind a foreground mass concentration or "lens," usually a galaxy. Because of the gravitational deflection of light rays by the lens, the observer sees multiple images of the quasar separated by a few arcseconds. Of order 10 unambiguous examples of multiply imaged quasars have been discovered so far, and they can be broadly classified into two kinds; those with two images of the quasar and those with four. We refer to the former as "doubles" and the latter as "quadruples." The only example that does not fit this classification is Q2016+112, which apparently has three images (Lawrence et al. 1984; Heflin et al. 1991). The interpretation of this object is confusing, however, (for instance, Narasimha, Subramanian, & Chitre 1987 propose that it is a quadruple with two of the images unresolved), and we do not include it in our considerations.

Theoretical studies of multiply imaged quasars have generally taken two approaches. In one approach, detailed models of individual examples of lensing are developed using realistic galaxy-like elliptical mass distributions (e.g., Narasimha, Subramanian, & Chitre 1982, 1987; Surdej et al. 1988; Kayser et al. 1990; Falco, Gorenstein, & Shapiro 1991; Kochanek 1991a). The models, which are adjusted to fit the positions and magnifications of the various observed images, provide useful information on the particular lenses, such as their masses and mass-to-light ratios. The models may also be combined with a measurement of time delay to derive important cosmographic parameters such as the Hubble constant (Falco et al. 1991; Kochanek 1991c; Narayan 1991).

The alternative approach to multiply imaged quasars is to consider the sample of lensed quasars as a whole and to derive statistical information about the lenses. In particular, one would like to know whether the observations are consistent with what one expects for lensing by the known populations of galaxies. Such studies generally use simplified models of lens potentials with a small number of parameters. The majority of work in this area has been limited to circularly symmetric isothermal mass distributions described by just one parameter, viz., the velocity dispersion (Gott & Gunn 1974; Hacyan 1982; Tyson 1983; Turner, Ostriker, & Gott 1984; Hinshaw & Krauss 1987; Narayan & White 1988; Wu 1989; Fukugita & Turner 1991; Mao 1991). The general conclusion of these studies is that the observed incidence of lensing is approximately consistent with that expected for the known galaxies in the universe, but that the image separations in some examples are larger than expected. The latter effect may be due to the additional deflection introduced by galaxy groups and clusters.

An important result from statistical studies is the identification of "magnification bias" in flux-limited samples (Turner 1980; Turner et al. 1984; cf. also Gott & Gunn 1974), which leads to an enhancement of the number of lensed quasars whenever the source counts increase toward fainter magnitudes. This bias arises because gravitational lensing generally leads to a magnification of the total flux received from a quasar. Consequently, at a given magnitude limit, the lensed quasars typically belong to an intrinsically weaker, and hence more numerous, population than the unlensed quasars.

Simple theoretical considerations (e.g., Narayan & Grossman 1989; Blandford et al. 1989), as well as detailed models of individual multiply imaged quasars, clearly indicate that it is important to include the ellipticity of the lens for realistic modeling. In particular, it is well known that one cannot produce quadruples with a purely circularly symmetric lens. Despite this, very few statistical investigations have included ellipticity in the analysis. The only detailed studies so far have been by Blandford & Kochanek (1987b), Kochanek & Blandford (1987), and Kochanek (1991b). These authors classified different kinds of doubles and quadruples and considered the relative numbers of these expected in the presence of various selection effects.

Apart from the velocity dispersion and ellipticity, a simple

lens requires one additional parameter to complete its description, viz., its core radius. The influence of the core radius has been investigated in a few studies involving circularly symmetric lenses (Narayan, Blandford, & Nityananda 1984; Hinshaw & Krauss 1987; Narayan & Schneider 1990) and in the papers mentioned above on elliptical lenses. We consider the role of this parameter in greater detail in this paper.

We present in § 2 a systematic analysis of the influence of core radius on lensing cross sections of elliptical lenses. We review some well-known theoretical results, and compute accurate cross sections for a wide range of lens parameters and magnifications. In § 3 we study the population of lenses in the universe, using galaxy data to model the distributions of velocity dispersion and ellipticity. The observations do not provide estimates of the core radius, which we therefore treat as a free parameter. In § 4 we present a composite model of the quasar luminosity function that extends up to redshift $z = 5$, and discuss the effect of lensing on this quasar population. In § 5 we combine our cross sections, lens distributions, and quasar luminosity function, to compute the distribution of lensed quasars as predicted by the model. We compare the predictions with the observations and conclude that lens core radii must be less than a few hundred parsecs. We summarize our conclusions in § 6.

2. CROSS SECTIONS

We have made detailed calculations of the cross section for gravitational lensing as a function of core radius and ellipticity, adopting an elliptical potential model for the deflector. The cross section, $\sigma_n(>\mu)$, represents the angular area in the plane of the source which will produce n images having a total magnification greater than a threshold magnification μ. The area is normalized by the square of the Einstein radius, θ_E^2.

2.1. *Lens Model*

We model an elliptical lens by means of a two-dimensional generalization of an isothermal potential of the form (Blandford & Kochanek 1987b)

$$\Phi(\xi_1, \xi_2) = 2\pi\sigma^2[\xi_c^2 + (1-\epsilon)\xi_1^2 + (1+\epsilon)\xi_2^2]^{1/2}, \quad (2.1)$$

where ξ_1, ξ_2 are linear coordinates in the lens plane, ξ_c is the linear core radius of the lens, σ is the one-dimensional velocity dispersion, and ϵ is the ellipticity. Ideally, we would like to model the mass density of the lens and use this to calculate the corresponding potential. Unfortunately there is no simple nonspherical density model that leads to an analytically tractable potential. We therefore choose to model the potential directly, so that we may employ a relatively simple set of equations (eqs. [2.5] and [2.6] below) to model the lensing. The surface mass density corresponding to the potential (eq. [2.1]) can be obtained using Poisson's equation. This derived density has a nearly elliptical profile for small potential ellipticities, $\epsilon < 0.2$. Therefore, we feel that the model in equation (2.1) is physically reasonable.

We convert equation (2.1) to angular coordinates using the angular diameter distances D_d, D_s, and D_{ds} between the observer and the lens (or deflector), the observer and the source, and the lens and the source, respectively, and assuming an Einstein–de Sitter universe. We scale all quantities by the Einstein radius, θ_E, of the lens, which refers to the angular radius of the ring image that would be formed if a point source were perfectly aligned with a circularly symmetric lens, i.e.,

$$\theta_E = 4\pi \frac{\sigma^2}{c^2} \frac{D_{ds}}{D_s}, \quad (2.2)$$

where c is the speed of light. In the case of an elliptical lens, one does not obtain an Einstein ring image for a point source at any position, but θ_E is nevertheless a useful scaling quantity.

We define scaled angular coordinates in the lens plane by $x_1 = \xi_1/D_d\theta_E$, $x_2 = \xi_2/D_d\theta_E$, $\boldsymbol{x} = (x_1, x_2)$, and angular coordinates in the source plane by $y_1 = \eta_1/D_s\theta_E$, $y_2 = \eta_2/D_s\theta_E$, $\boldsymbol{y} = (y_1, y_2)$, where η_1, η_2 are linear coordinates in the source plane. The lens equation then gives

$$\boldsymbol{y} = \boldsymbol{x} - \frac{2}{c^2}\nabla\Phi\frac{D_{ds}}{D_s}. \quad (2.3)$$

Defining also a scaled angular core radius,

$$x_c = \xi_c/\theta_E D_d, \quad (2.4)$$

and substituting in equation (2.1), we obtain the following dimensionless equations:

$$y_1 = x_1 - \frac{(1-\epsilon)x_1}{[x_c^2 + (1-\epsilon)x_1^2 + (1+\epsilon)x_2^2]^{1/2}}, \quad (2.5)$$

$$y_2 = x_2 - \frac{(1+\epsilon)x_2}{[x_c^2 + (1-\epsilon)x_1^2 + (1+\epsilon)x_2^2]^{1/2}}. \quad (2.6)$$

For a given source position (y_1, y_2), equations (2.5) and (2.6) may be solved to obtain the positions (x_1, x_2) of all the images. Once these positions are known, the magnifications of the images, μ, can be calculated using

$$\mu = \left| \frac{\partial y_1}{\partial x_1}\frac{\partial y_2}{\partial x_2} - \frac{\partial y_1}{\partial x_2}\frac{\partial y_2}{\partial x_1} \right|^{-1}. \quad (2.7)$$

Thus the positions and magnifications of the images corresponding to any point source are completely determined once the following three parameters of the lens are given: the Einstein radius of the lens, θ_E (or, equivalently, the velocity dispersion σ), the ellipticity of the lens, ϵ, and the angular core radius, x_c.

2.2. *Image Multiplicities and Caustics*

We briefly review here the properties of elliptical lenses as a function of core radius, focusing in particular on the various image multiplicities n that are possible. These theoretical results are known to specialists in the field but have not been explicitly described before.

Figure 1 shows a sequence of lens configurations with core radius increasing to the right. As can be seen, the areas in the source plane corresponding to different multiplicities n vary with the lens core radius. In the first three panels of Figure 1 the most central region of the source plane produces five images, the area on the outside produces one image, and the intermediate regions produce three images. The lines separating regions of different multiplicity are called caustics. These come in two varieties: fold caustics, which appear as lines, and cusp caustics, which are points where two folds come together.

If the dimensionless core radius x_c is sufficiently small, the caustic framing the five-image region has four cusps and is completely detached from the outer, purely fold caustic (Fig. 1*a*). The inner caustic in this case is referred to as the "astroid caustic" or the "tangential caustic," while the outer caustic is

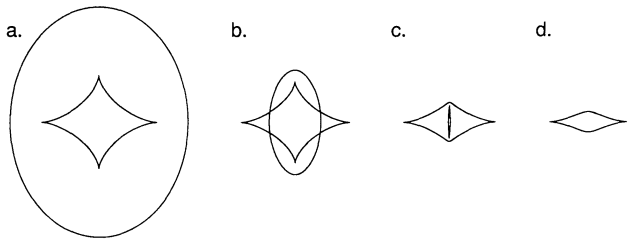

FIG. 1.—Evolution of caustic structure with increasing core radius for an elliptical lens with $\epsilon = 0.2$. Core radius increases from left to right and has values of $x_c = \xi_c/D_d\theta_E = 0.05$, 0.4, 0.75, and 0.9, respectively. In (*a*), (*b*), and (*c*) the central region is the area of the source plane which produces five images, the outermost region produces one image, and the intermediate regions produce three images. In (*d*) the regions inside and outside the caustic produce three images and one image, respectively. The critical core radii corresponding to transitions from one configuration to the next are listed in Table 1.

called the "radial caustic." With increasing core radius, two of the inner cusps push through the shrinking outer fold caustic to produce the configuration shown in Figure 1*b*. This happens when x_c crosses a critical value c_1, which depends on the lens ellipticity (Table 1).

Still larger core radii give rise to an elongated five-image region which detaches from the three-image region, leaving two doubly cusped "lips caustics" (Fig. 1*c*). The transition to this configuration occurs when $x_c = c_2$. As the core radius increases further, the five-image region shrinks until it disappears altogether at $x_c = c_3 = 1 - \epsilon$, leaving behind the case shown in Figure 1*d*. The remaining lips caustic, too, continues to shrink with increased core radius until it finally disappears when $x_c = c_4 = 1 + \epsilon$. For $x_c > c_4$, no multiple images are possible for any source position. Table 1 lists the values of the four critical core radii c_1, c_2, c_3, and c_4 for various values of ϵ.

The caustics separating regions of different image multiplicity are important for statistical studies because sources that are located in their vicinity have highly brightened images. Caustics, therefore, have a large effect on the cross sections for lensing, particularly at high magnification. For a point source on the higher multiplicity side of a fold caustic, one pair of images is highly brightened, with magnifications varying inversely as the square root of the source offset from the caustic. As the source crosses the caustic, this pair of images merges and becomes infinitely bright before disappearing instantaneously as the source moves into the lower multiplicity region. It can be shown that for a fold caustic the area near the caustic producing images brighter than magnification μ, i.e., the cross section $\sigma(>\mu)$, scales as μ^{-2}.

For sources on the higher multiplicity side of a cusp caustic there are three highly magnified images which merge into one as the source crosses the caustic into the lower multiplicity region. The remaining image in this case continues to be highly magnified. Thus cusps can produce greatly magnified images both inside and outside the caustic. This implies that even singly imaged point sources can be greatly magnified if they lie just outside a cusp. The cross section, $\sigma(>\mu)$, for a cusp caustic scales as $\mu^{-5/2}$ for large μ.

Figure 2 shows examples of sources and their images inside and outside caustics. The dotted lines represent critical lines, i.e., the loci of points on which brightened image pairs merge as their magnifications become infinite, and the sizes of the symbols in the image plane indicate qualitatively the relative magnifications of the images. Notice that the central image is generally dimmer than the other images. This is reflected in the observations of multiply imaged quasars, where the central image has not been detected in any of the examples. Therefore, configurations that we refer to as having three or five images in the simulations refer in fact to cases with two or four images in the observations, i.e., to "doubles" and "quadruples," respectively.

TABLE 1

CRITICAL CORE RADII

ϵ	c_1	c_2	c_3	c_4
0.05	0.70146	0.90363	0.95	1.05
0.10	0.48051	0.81408	0.90	1.10
0.15	0.31246	0.73077	0.85	1.15
0.20	0.18372	0.65320	0.80	1.20

2.3. *Computation of Cross Sections*

We have computed the cross sections $\sigma_n(>\mu)$ associated with n images having total magnification greater than μ for various choices of n, μ, x_c, and ϵ. The cross sections are expressed in units of θ_E^2. The contours of constant magnification around any one of our caustic configurations are extremely complex, therefore the cross sections were computed using a numerical scheme similar to that described by Blandford & Kochanek (1987b).

The target magnifications we considered are $\mu = 2^N$ for $N = 1$–10. At the highest magnification, $\mu = 2^{10} = 1024$, the cross sections are very small, but we have nevertheless been able to obtain relatively noise-free results over the entire range of μ. The cross sections were calculated for 139 equally spaced values of the core radius from $x_c = 0.025$ up to 3.475, beyond which the total magnification never exceeds our minimum target magnification of 2. The entire calculation was repeated for five values of the lens ellipticity: $\epsilon = 0$, 0.05, 0.1, 0.15, and 0.2.

Figure 3 shows the total cross section, $\sigma_n(>\mu)$, as a function of core radius for $\epsilon = 0.2$. The influence of the various critical core radii mentioned in § 2.2 may be seen. For instance, three images are produced only for $x_c < c_4 = 1 + \epsilon$, and five images only for $x_c < c_3 = 1 - \epsilon$. Singly imaged sources have significant magnifications only for x_c lying between c_1 and c_4, as this is the core radius range over which a cusp caustic penetrates into the single-image region (Fig. 1). The first critical point, $c_1 = 0.184$, corresponds to noticeable fluctuations in the high-magnification cross sections of the multiplicity 3 and 5 plots. The second critical point, $c_2 = 0.653$, where the five-image region separates from the three-image region (Fig. 1*c*), also produces fluctuations in the cross sections of multiply imaged cases.

It is clearly seen from Figure 3 that the cross sections corresponding to $\mu = 2^N$ are evenly spaced as a function of N on a logarithmic scale. This is due to the power-law behavior of cross section as a function of magnification near a caustic (cf. § 2.2). These plots can therefore be extrapolated to infinitely high magnifications using the theoretical scaling laws. Remembering that cross sections near a cusp scale as $\mu^{-2.5}$, it is clear that the single-image cross section must have a -2.5 power law for all those core radii for which there are high magnifications ($c_1 < x_c < c_4$). Similarly, the five-image cross section scales always as μ^{-2}, since it is influenced only by the inside of folds (Figs. 1*a*–1*c*), the inside of the cusp having a negligible effect in this case.

The three-image case is more complex, since this region of

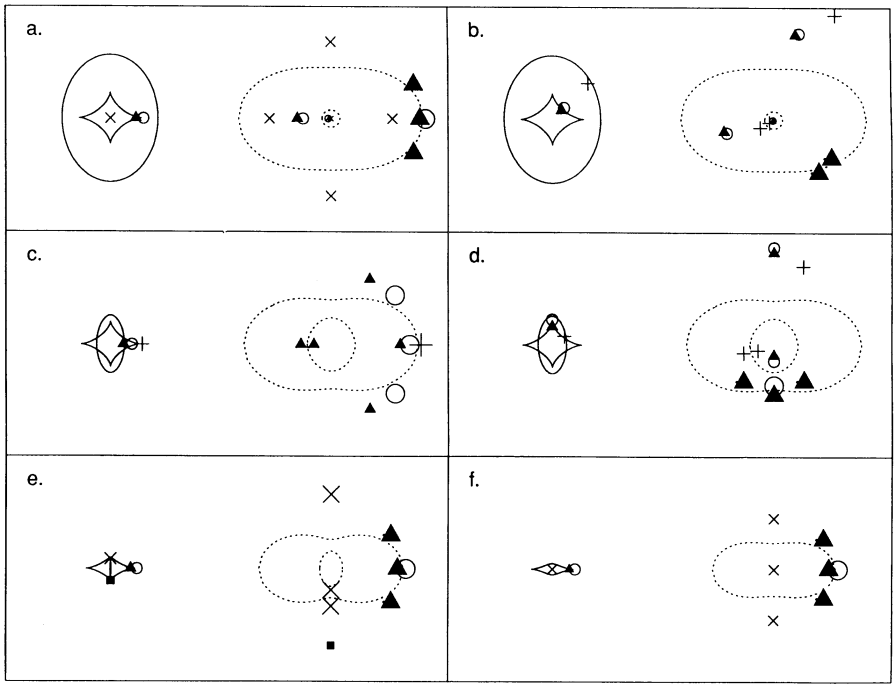

FIG. 2.—Examples of multiple imaging of point sources by an elliptical lens with core radii corresponding to the four cases shown in Fig. 1. Panels *a* and *b* correspond to a lens with $x_c = 0.05$, panels *c* and *d* have $x_c = 0.4$, panel *e* has $x_c = 0.75$, and panel *f* corresponds to $x_c = 0.9$. In each panel, the left half represents the source plane, in which the solid lines are caustics, and the symbols represent the positions of point sources. The right half of each panel shows the image plane, in which the dotted lines are the critical curves, and the symbols indicate the positions of the images. The relative sizes of the image symbols indicate qualitatively their magnifications. Sources which lie just inside a fold caustic or close to a cusp caustic have some images which are highly brightened and converging on a critical line. As the source crosses a caustic into a lower multiplicity region, two bright images disappear. Notice the demagnification of the central image in panels *a* and *b*.

the source plane can be influenced by both the outside of cusps and the inside of folds. For small core radii (Fig. 1*a*) the cusp power law dominates at moderate magnifications, and so the cross section scales as $\mu^{-2.5}$. At very large μ, beyond the values we have considered, the fold caustics will take over and the cross section will flatten to a μ^{-2} dependence. The magnification at which this transition occurs decreases as the core radius increases. Roughly, for $x_c > c_1$, the influence of the fold dominates for all magnifications.

3. LENS POPULATION

We concentrate exclusively on galaxy lenses in this paper. For these we can use the observations to select appropriate values for the lens parameters. As described in the previous section, we model the projected lens potential by means of three parameters: the Einstein radius, θ_E; the angular core radius, x_c; and the potential ellipticity, ϵ. These quantities are functions of three physical parameters of the lens: the velocity dispersion, σ; the linear core radius, ξ_c; and the mass ellipticity, γ. We can use the observations to get some idea of the values of these parameters.

For the distribution of σ, we follow Fukugita & Turner (1991) and use the Faber-Jackson relation to estimate σ in terms of the galaxy luminosity, L. Thus we have $\sigma = (L/L_*)^{1/4}\sigma_*$, with L assumed to follow a Schechter luminosity function. We have separately considered elliptical, S0, and spiral galaxies using Fukugita & Turner's formulae to relate σ directly to blue magnitudes.

For the distribution of ellipticities we used the data of Huchra et al. (1983), which contains magnitudes, redshifts, galaxy types, and isophotal axis ratios for 2300 galaxies from the redshift survey. Figure 4 shows histograms of the observed isophotal ellipticities, γ, for the three galaxy types we have considered. As discussed in § 2.1, the elliptical potential we use corresponds to a roughly elliptical mass density for small ϵ. If we define the ellipticity, γ_m, of the surface mass density to be 1 minus the mass axis ratio, then for $x \gg x_c$ we find

$$\gamma_m \simeq 1 - \left(\frac{1-\epsilon}{1+\epsilon}\right)^{3/2} . \tag{3.1}$$

Assuming that light traces mass, we can set γ_m equal to the observed isophotal γ. Using equation (3.1), we can then estimate the ranges of γ corresponding to our five model ellipticity bins centered on $\epsilon = 0$, 0.05, 0.1, 0.15, and 0.2. The boundaries of the five bins are indicated by dotted lines in Figure 4.

Considering next the linear core radius, ξ_c, we notice that the dimensionless core radius x_c is proportional to ξ_c/σ^2. We make the simplifying assumption that $\xi_c \propto \sigma^2$ for the entire population of lenses, i.e.,

$$\xi_c = \left(\frac{\sigma}{\sigma_*}\right)^2 \xi_c^* . \tag{3.2}$$

Thus one parameter, ξ_c^*, controls the core radii of all the model lenses. Once ξ_c^* is selected, all lenses have the same x_c for a given source and lens redshift. We adopt a range of ξ_c^* values in our computations, and present results for $\xi_c^* = 100$, 300, and 1000 pc. Note that Fukugita & Turner (1991) employed a core radius scaling of the form $\xi_c \propto \sigma^{4.8}$ based on measured core radii of a few nearby galaxies (Lauer 1985), while Kochanek (1991b) examined three different scalings: ξ_c = constant, $\xi_c \propto \sigma^2$, and $\xi_c \propto \sigma^{4.8}$.

Turner et al. (1984) and Fukugita & Turner (1991) introduced a parameter F which describes the effectiveness of a

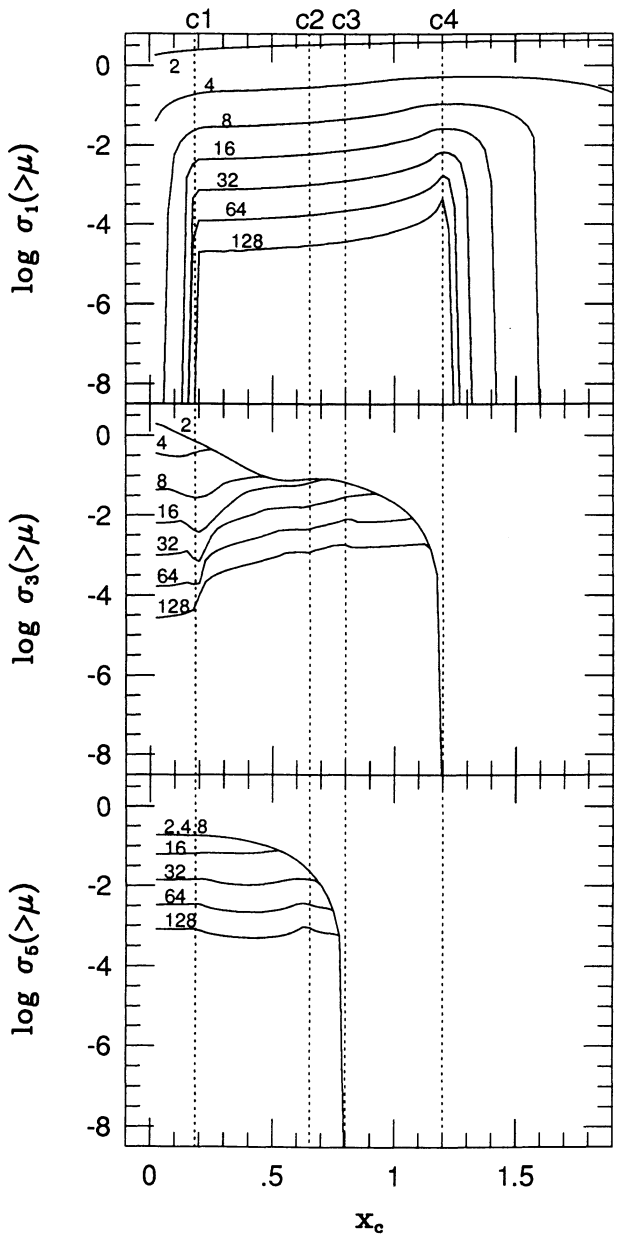

FIG. 3.—Cross sections for lensing by an $\epsilon = 0.2$ lens as a function of lens core radius x_c. Each curve represents the cross section for lensing with total magnification greater than a given magnification μ. The magnification for each curve is labeled on the plot. The vertical lines indicate the positions of critical core radii c_1, c_2, c_3, c_4, where the caustic configuration in the source plane undergoes a qualitative change.

cosmologically distributed population of isothermal spheres in producing multiple images, defined as

$$F = \frac{16\pi^3}{cH_0^3} \langle n_0 \sigma^4 \rangle . \tag{3.3}$$

We have estimated F corresponding to each galaxy type and ellipticity range using the data of Huchra et al. (1983) by summing over the galaxies according to

$$\langle n_0 \sigma^4 \rangle = \sum_i \frac{\sigma_i^4}{(4/3)\pi d_i^3 f} . \tag{3.4}$$

Here d_i is the limiting distance to which the ith galaxy could have been seen at the magnitude limit of the survey, and f represents the fraction of the sky that was sampled. A value of $H_0 = 100$ km s^{-1} Mpc^{-1} was assumed for the Hubble constant. The velocity dispersion, σ_i, of the ith galaxy is estimated using the Faber-Jackson relation, but includes an additional factor of $(3/2)^{1/2}$ in the case of elliptical and SO galaxies (Turner et al. 1984; Fukugita & Turner 1991). The correction factor takes into account the velocity dispersion of the dark matter which presumably dominates these galaxies. The results of these calculations are given in Table 2. The total value of F for all galaxies is 0.066, which is about 50% larger than the value used by Fukugita & Turner (1991) and Kochanek (1991b). This discrepancy may be due in part to the fact that

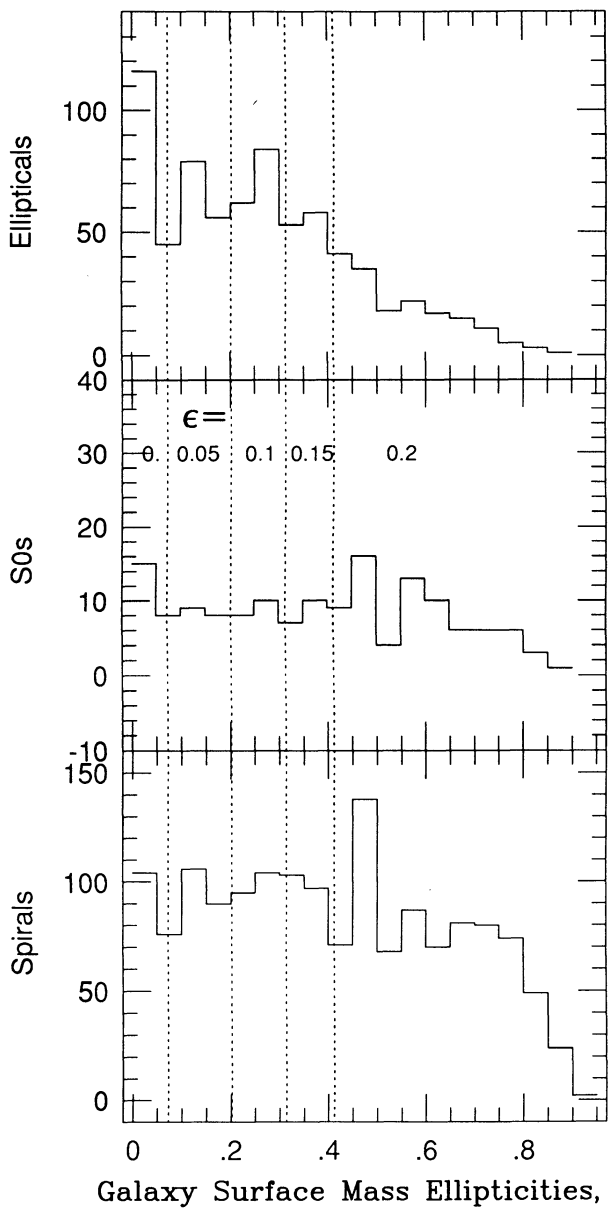

FIG. 4.—Distribution of ellipticities of galaxies in the redshift survey of Huchra et al. (1983), shown according to galaxy type. The vertical lines indicate the boundaries separating the five bins of ϵ (potential ellipticity), for which the model computations were done.

TABLE 2

WEIGHTS F BY GALAXY TYPE AND ELLIPTICITY

Type	$\epsilon = 0.0$	$\epsilon = 0.05$	$\epsilon = 0.10$	$\epsilon = 0.15$	$\epsilon = 0.20$	Total
Spiral	4.8E−04	7.9E−04	6.1E−04	4.7E−04	2.2E−03	4.6E−03
S0	4.0E−03	5.6E−03	1.2E−02	3.2E−03	1.4E−02	3.9E−02
Elliptical	5.2E−03	5.2E−03	8.1E−03	2.8E−03	1.7E−03	2.3E−02
Total	9.7E−03	1.2E−02	2.1E−02	6.5E−03	1.8E−02	6.6E−02

the Huchra et al. survey is dominated by the local supercluster (E. Turner, private communication).

4. QUASAR LENSING

4.1. *The Quasar Luminosity Function*

We are ultimately interested in what will be observed upon looking out into a universe containing a population of quasars being lensed by the population of galaxy lenses described in the previous section. First, however, we develop a model of the quasar distribution.

Boyle, Shanks, & Peterson (1988) have published a sample of over 400 faint, ultraviolet-excess quasars that extends from $z = 0.3$ out to $z = 2.2$ and is complete for magnitudes brighter than 20.9 mag. Using this sample, they proposed a quasar luminosity function of the form

$$\Phi(z, M_B) = \frac{\Phi^*}{10^{0.4[M_B - M_B(z)](\alpha+1)} + 10^{0.4[M_B - M_B(z)](\beta+1)}} \quad \text{Mpc}^{-3}\ \text{mag}^{-1}. \quad (4.1)$$

$M_B(z)$, the magnitude at which there is a turnover in the power-law slope, varies as a function of quasar redshift:

$$M_B(z) = M_B^* - 2.5k_L \log (1 + z)\,, \quad (4.2)$$

where M_B^* and k_L, as well as α and β from equation (4.1), are constants given by the best fit of the parameters to the data. We have used model B from Boyle et al. (1988), a pure power-law evolution that fits the data very well. For this model, the values of the constants are $M_B^* = -22.42$, $k_L = 3.15$, $\alpha = -3.79$, $\beta = -1.44$, and $\Phi^* = 7.8 \times 10^{-10}$.

The Boyle et al. model is valid only out to $z = 2.2$, and there is no general consensus yet on the form of the luminosity function at higher redshift. Using recent papers by Schmidt, Schneider, & Gunn (1992), Warren, Hewitt, & Osmer (1992), and Irwin, McMahon, & Hazard (1992) as a guide, we have developed a hybrid model in which the Boyle function continues out to $z = 2.5$ and is then flat out to $z = 3$. Above $z = 3$, we assume that the luminosity function falls by a factor of 3.2 per unit redshift for intermediate magnitudes while staying constant at bright magnitudes. Thus, for $z > 3$, we adopt

$$\Phi(z, M_B) = \frac{\Phi^* \times 10^{-\{A + B[0.4(\beta+1)]\}}}{10^{0.4[M_B - M_B(z)](\alpha+1)} + 10^{0.4[M_B - M_B(z)](\beta+1)}} \quad \text{Mpc}^{-3}\ \text{mag}^{-1}, \quad (4.3)$$

with

$$A = (z - 3) \log 3.2\,, \quad (4.4)$$

$$M_B(z) = M_B^* - 2.5k_L \log (1 + z) + B\,, \quad (4.5)$$

$$B = \frac{A}{0.4(\alpha - \beta)}\,. \quad (4.6)$$

Figure 5 shows our composite luminosity function for a range of redshifts. We assume that there are no quasars beyond a redshift of 5.

Integrating the luminosity function over redshift and magnitude, we can predict the number of quasars that should be observed as a function of the apparent magnitude limit of a survey. The results are shown in Figure 6 for both the Boyle et al. model alone, which extends from $z = 0.3$ to $z = 2.2$, and our composite model, which continues to $z = 5$.

4.2. *The Effect of Lensing*

We now include galaxy lenses and ask how they affect a magnitude-limited sample of quasars. We will consider a quasar to be "lensed" if it either has multiple images or is singly imaged with a magnification $\mu \geq 2$. In computing the number of lensed quasars, $N_{\rm LQ}(<m_B)$, it is convenient to distinguish between two cases: (1) quasars which are bright enough to have been in the sample even if they had not been lensed and (2) quasars which are intrinsically too dim to be seen but as a result of lensing are brightened sufficiently to be included in the sample. We refer to the number of each of these as $N_{\rm LQ,\,BRI}(<m_B)$ and $N_{\rm LQ,\,DIM}(<m_B)$, respectively. The sum of these two components yields $N_{\rm LQ}(<m_B)$.

Consider first the quasars which were already brighter than the cutoff magnitude. For these we have

$$N_{\rm LQ,BRI}(<m_B) = \int_{0.3}^{5} w(z_s)dz_s \int_0^{z_s} w'(z_d, z_s)dz_d \times \int_{m_B=0}^{M_{\rm Lim}} \Phi(z_s, M_B)\sigma(\mu \geq 2)dM_B\,, \quad (4.7)$$

where $w(z_s)$ and $w'(z_d, z_s)$ are weighting functions. $M_{\rm lim}$ is the

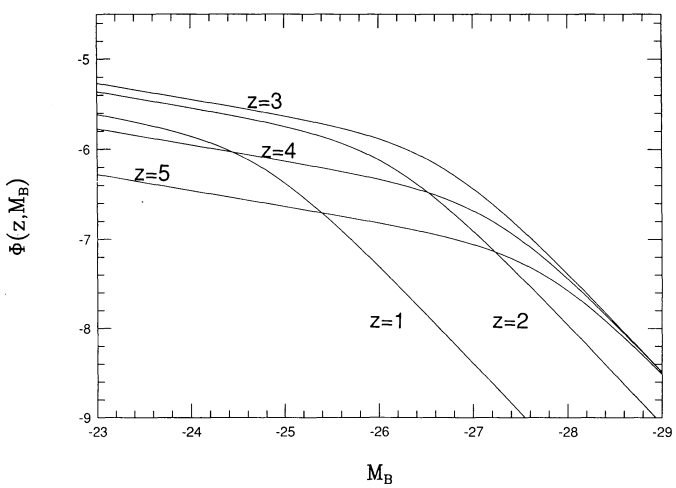

FIG. 5.—Model quasar luminosity function $\Phi(z, M_B)$ used in the calculations.

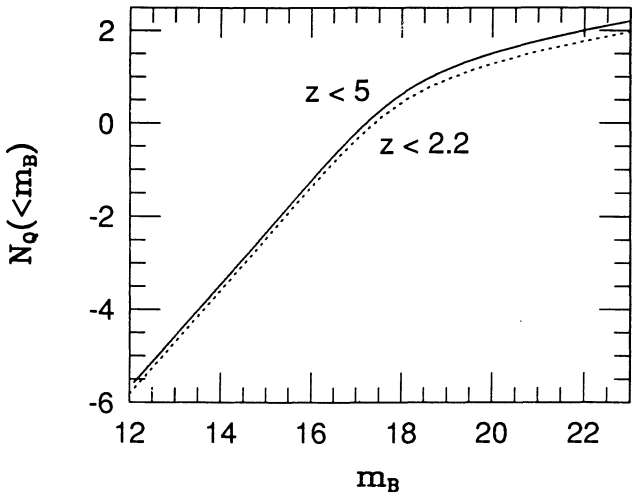

FIG. 6.—Quasar number counts (in the absence of lensing) per square degree. The dotted line shows the predicted number of quasars in a magnitude-limited sample using the luminosity function of Boyle et al. (1988) which extends only to $z = 2.2$. The solid line correspnds to our hybrid model (Fig. 5), which extends to $z = 5$.

absolute magnitude corresponding to the apparent magnitude cutoff of m_B. This takes into account the K-correction and cosmological effects, and is given by

$$M_{\rm lim} = m_B - 5 \log \{(2c/H_0)[(1 + z_s) - (1 + z_s)^{1/2}]/10 \text{ pc}\} + 1.25 \log (1 + z_s) . \quad (4.8)$$

The quasar weighting function $w(z_s)$ assumes a homogeneous comoving density of quasars, and the lens weighting function $w'(z_d, z_s)$ makes a similar assumption about the lenses. In addition, $w'(z_d, z_s)$ includes geometrical factors associated with the probability of obtaining a lensing event (see Turner et al. 1984 for details). The two functions are given by

$$w(z_s) = \frac{4c^3}{H_0^3} \frac{1}{(1 + z_s)^{3/2}} \left[1 - \frac{1}{(1 + z_s)^{1/2}}\right]^2 , \quad (4.9)$$

$$w'(z_d, z_s) = \frac{4F}{\pi} \frac{[(1 + z_d)^{1/2} - 1]^2[(1 + z_s)^{1/2} - (1 + z_d)^{1/2}]^2}{(1 + z_d)^{7/2}[(1 + z_s)^{1/2} - 1]^2} . \quad (4.10)$$

The integral over quasar redshifts in equation (4.7) goes from $z_s = 0.3$ to $z_s = 5$, the range over which our luminosity function is valid. The integration in lens redshift z_d, covers the space from the observer to the quasar. We integrate over quasar magnitude ranging from the faint cutoff limit of our sample up to an apparent magnitude of zero (sufficiently bright to include all sources). For each magnitude, we multiply the luminosity function by the cross section for lensing corresponding to $\mu = 2$. This is the area in the source plane which will produce any lensing at all, since $\mu = 2$ is the lowest net magnification that can be produced with multiple images and is also the cutoff magnification corresponding to our definition of "lensed" single images. For each z_s, z_d in equation (4.7), we compute the angular core radius x_c of the lenses corresponding to our adopted choice of ξ_c^* (eq. [3.2]), and we obtain $\sigma_n(\geq 2)$ for that core radius from the data described in § 2.3. The computations were done for a range of core radii ξ_c^*, in each case considering independently the three multiplicities $n = 1, 3, 5$.

The second half of the calculation looks at quasars that are intrinsically dimmer than m_B but are brightened enough by lensing to be included in the survey. For these we have

$$N_{\rm LQ,DIM}(<m_B) = \int_{0.3}^{5} w(z_s)dz_s \int_0^{z_s} w'(z_d, z_s)dz_d \times \int_{M_{\rm lim}}^{M_{\rm lim}+12.5} \Phi(z, M_B)\sigma(\mu \geq \mu_c)dM_B . \quad (4.11)$$

The z integrals are the same as in the previous calculation, but now the limits on the magnitude integral run from the cutoff magnitude to 12.5 mag fainter (the upper limit corresponds to $\mu = 10^5$, which we consider a safe limit). Quasars in this magnitude range could not be observed without lensing. At each magnitude M, we use the cross section corresponding to magnification $\mu = \mu_c$, where μ_c is the magnification necessary to bring a quasar of absolute magnitude M and redshift z_s up to the limiting apparent magnitude, m_B,

$$\mu_c = 10^{0.4(M - M_{\rm lim})} . \quad (4.12)$$

Combining $N_{\rm LQ,\,BRI}(<m_B)$ and $N_{\rm LQ,\,DIM}(<m_B)$ we obtain $N_{\rm LQ}(<m_B)$, which represents the total number of quasars in a magnitude-limited sample brighter than m_B which have been affected by lensing.

5. RESULTS AND DISCUSSION

5.1. *Number Counts of Lensed Quasars*

Figure 7 shows plots of $N_{\rm LQ}(<m_B)$ corresponding to multiplicities of 1, 3, and 5. For comparison, the unlensed number counts $N_Q(<m_B)$ are also shown as dotted lines. The top panel of Figure 7 corresponds to a small linear core radius, $\xi_c^* = 100$ pc; the middle panel to an intermediate core radius, $\xi_c^* = 300$ pc; and the bottom panel to a large core radius $\xi_c^* = 1000$ pc. The influence of ξ_c^* on lens cross sections is readily seen from these diagrams.

All three multiplicities have identical slopes of $\log N_{\rm LQ}(<m_B)$ versus m_B at faint magnitudes, the same as that of the unlensed counts. At bright magnitudes, however, the slopes differ. When the core radius is small (Fig. 7, *top*), x_c is smaller than c_1 for most of the range of lens and source redshift. In this regime, the cross section scales with magnification as $\mu^{-2.5}$ for three-image cases and as μ^{-2} for five-image cases (§ 2.2). These scalings yield slopes of 1 and 0.8 in Figure 7. Note the interesting feature that we expect more quintuply imaged sources than triply imaged ones at very bright magnitudes, since the cross section for triply imaged cases falls off faster with μ. The slope of the single-image curve in the top panel of Figure 7 is steeper than the three or five-image curves because, for low x_c, there are no highly magnified single images at all (Fig. 1 and § 2.2). Therefore, this curve lies essentially parallel to the unlensed curve. These results agree very well with similar calculations done by Kochanek (1991b).

For a large linear core radius of 1000 pc (Fig. 7, *bottom*), the angular radius x_c ranges over all the different configurations shown in Figure 1 as the lens redshift z_d varies. Consequently, in this case, there is a significant probability for single images to be highly brightened because of the presence of a cusp. Since the cross section scales as $\mu^{-2.5}$, the $N_{\rm LQ}(<m_B)$ curve for $n = 1$ has a slope of 1. Further, in this regime the cross sections for both $n = 3$ and $n = 5$ scale as μ^{-2}, giving a slope of 0.8 in the bottom panel of Figure 7 (cf. § 2.2). In fact, the two curves turn out to be very close to each other over the entire magnitude

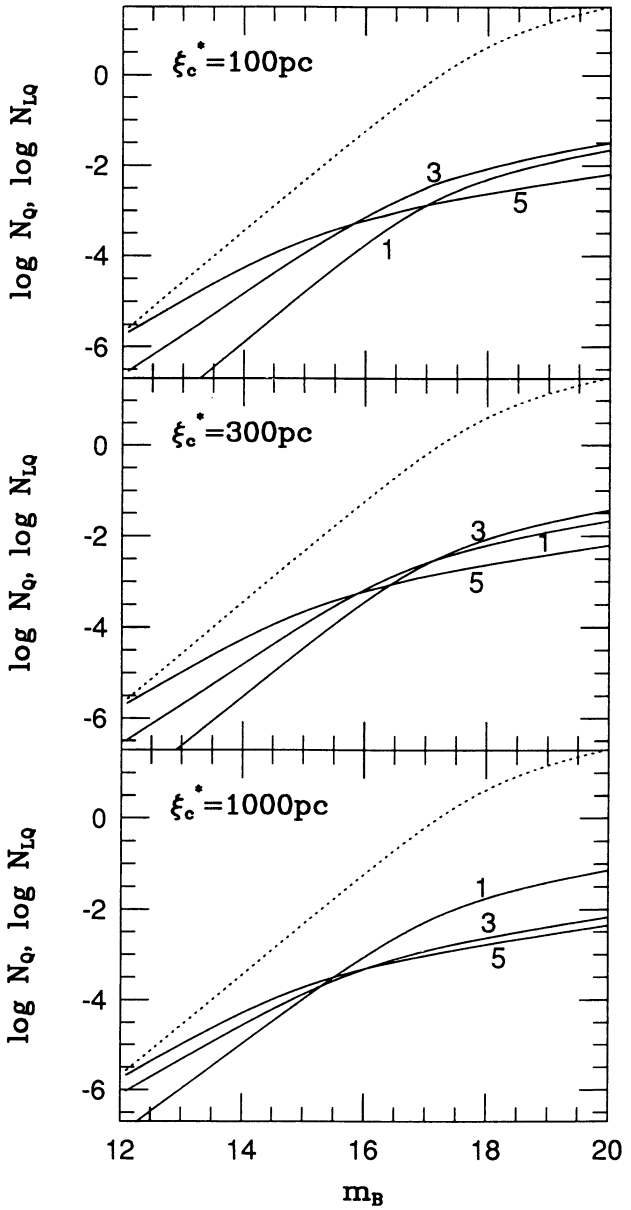

FIG. 7.—Cumulative number counts of lensed and unlensed quasars for three values of the linear core radius: $\xi_c^* = 100$, 300, and 1000 pc. The dotted line in each panel shows the number of quasars brighter than a given magnitude, m_B. The solid lines give the predicted numbers of lensed quasars corresponding to each image multiplicity. The slopes of the various curves differ because of the influence of caustics in the source plane (see the text for details).

range. The intermediate core radius case (Fig. 7, *middle*) shows features in between the two extremes.

5.2. *Magnification Bias*

One important aspect of our results is that they allow us to estimate the magnification bias (Turner 1980; Turner et al. 1984; Fukugita & Turner 1991), which is a measure of the excess of lensed sources in flux-limited samples caused by magnification. In § 4.2 we calculated the number of quasars brighter than a certain magnitude cutoff which undergo lensing and called it $N_{\rm LQ,\,BRI}(<m_B)$. This is the number of lensed quasars one would naively estimate to be discovered in a survey. The total number of lensed quasars, however, is the sum of $N_{\rm LQ,\,BRI}(<m_B)$ and $N_{\rm LQ,\,DIM}(<m_B)$, the latter quantity describing the number of quasars dimmer than the magnitude cutoff which are brought into the survey through lens magnification. The bias factor, $B(<m_B)$, measures the overrepresentation of lensed sources due to this effect, and is defined to be

$$B(<m_B) = \frac{N_{\rm LQ,\,BRI}(<m_B) + N_{\rm LQ,\,DIM}(<m_B)}{N_{\rm LQ,\,BRI}(<m_B)} . \qquad (5.1)$$

Biases become particularly large when the intrinsic luminosity function is steep.

The bias factors calculated with our models for various lens multiplicities are shown in Figure 8 for $\xi_c^* = 100$, 300, and 1000 pc. Note how extremely high the bias is at bright magni-

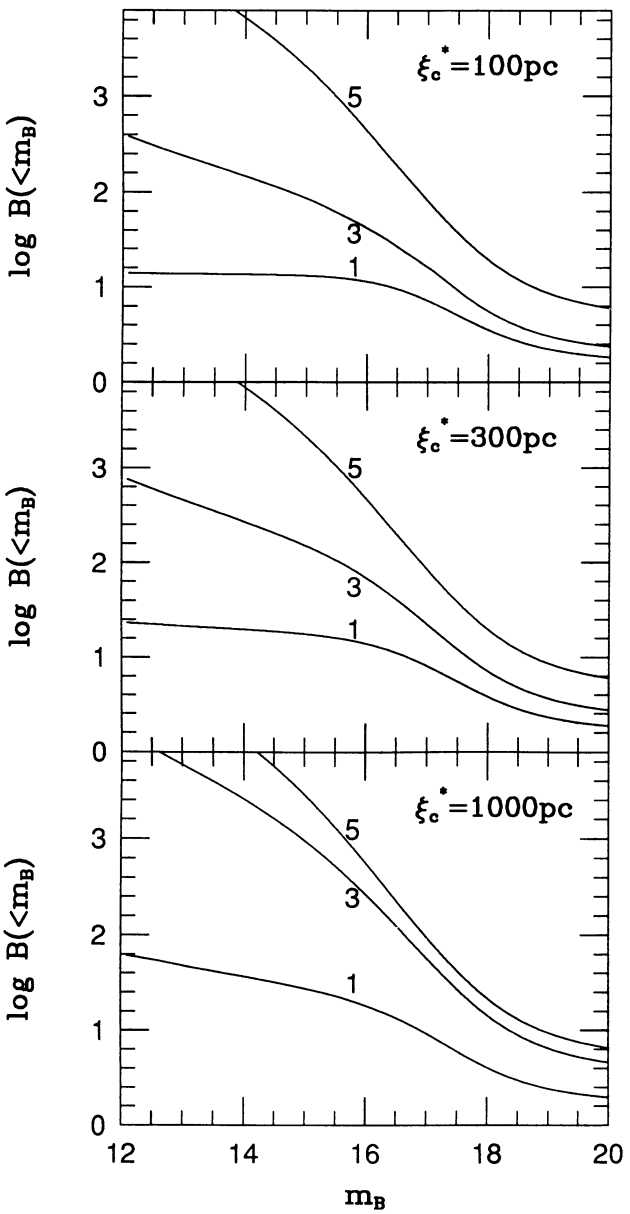

FIG. 8.—Magnification bias factor $B(<m_B)$ due to an elliptical lens for three values of the lens core radius: $\xi_c^* = 100$, 300, and 1000 pc. Five-image cases have a particularly high bias at bright magnitudes, and are overrepresented by a factor of 5 even at faint magnitudes.

tudes. Since the bias is a result of high magnifications, it is strongly affected by the properties of caustics. Just as the slopes of the number counts vary with different multiplicities as a result of the underlying caustic structure, the biases also show similar variations. Our results for one and three images with $x_c = 100$ pc agree very closely with those of Turner & Fukugita (1991), who calculated biases for a population of singular isothermal spheres. Their spherical models, however, produce no more than three images, and so they miss the huge bias in the case of five images that we find. For larger core radii, the biases for the one- and three-image cases increase significantly, with the three-image bias becoming nearly as large as that for the five-image case.

The influence of magnification bias can be clearly seen in the observations. Excluding the problematical Q2016+112, the five most secure cases of lensing all have magnitudes brighter than about 17 mag. The sources Q0957+561, Q0142−100, H1413+117, and Q2237+031 have $m_V \sim 17$, and Q1115+080 has $m_V \sim 16$. Even if we include the handful of other, less reliable and fainter lens candidates, we still find that half the known optical lenses are brighter than 17 mag. On the other hand, the sample of known quasars peaks at around 19 mag (Hewitt & Burbidge 1987), with the vast majority being fainter than 17 mag. Similarly, the quasars that have been imaged with sufficient resolution to detect lensing extend down to 19 mag (at least) and are distinctly fainter than the lensed sample. Thus, there is a clear preponderance of bright quasars in the lens sample which is almost certainly a result of magnification bias. Our models show that for $\xi_c^* = 100$ pc the overrepresentation of lensed sources is a factor of ~ 15 for triply imaged cases and ~ 85 for five-image cases at $m_B = 17$ (~ 40 and ~ 400 at $m_B = 16$), as opposed to biases of only ~ 3 and ~ 8 at $m_B = 19$.

Among the five lensed quasars brighter than 17 mag listed above, we have roughly equal numbers of doubles and quadruples: Q0957+561 and Q0142−100 have two images each, and the others have four images. This too, is consistent with the model. Figure 7 shows that the number of three-image and five-image cases are about equal at $m_B \sim 16.5$.

Although the above features are generally true for all core radii we have tried, a quantitative comparison of the models and the data suggests that the core radii may be closer to 100 pc than to 1000 pc. First, the total probability of lensing has a modest dependence on core radius (as noted by Hinshaw & Krauss 1987). For $\xi_c^* = 100$ pc the fraction of 17 mag quasars expected to be multiply imaged is around 1 in 150 according to our models, while for $\xi_c^* = 1000$ pc the probability is reduced to about 1 in 350. The observed fraction of multiply imaged quasars is approximately 1 in 100. If the bulk of lensing in the universe is done by galaxies, then these numbers suggest that galaxy core radii are likely to be less than a few hundred parsecs.

Second, among the five or six lens candidates fainter than 17 mag, nearly all are doubles, and the only quadruple, viz., 0414+0534, is a radio-selected source. This suggests that doubles are much more common than quadruples at faint magnitudes. In our models, we predict that for $\xi_c^* = 100$ pc there will be 5 times as many doubles as quadruples at 20 mag, whereas for $\xi_c^* = 1000$ pc, we predict that doubles will be overrepresented by only $\sim 50\%$. This again suggests small core radii. However, the best evidence on core radii comes from the missing odd image in the observed multiply imaged quasars, as we discuss in the following section.

5.3. *Missing Image and Core Radius*

It is a well-known theoretical result that a gravitational lens should produce an odd number of images. In particular, the elliptical models we have considered should have either three or five images. Nevertheless, the observed examples are all either doubles or quadruples (2 or 4 images), the missing image in all cases being one that ought to have been found close to the center of the lens. The absence of the odd image has been hypothesized to be due in part to reddening, but is more likely explained as being the result of large demagnification by the core of the lens (Narayan et al. 1984). On this assumption, the absence of the central image should provide a constraint on the core radius of the lens.

We have explored this possibility in our calculations by monitoring an additional parameter, R, which represents the ratio of the magnifications of the brightest and dimmest images. We calculated all the cross sections described in § 2.3 as a function of both the total magnification μ and the ratio R, defining $\sigma_n(>\mu, >R)$ to be the cross section for total magnification greater than μ and magnification ratio greater than R. We calculated these cross sections over the entire range of x_c and ϵ for values of R equal to 1, $10^{0.5}$, 10^1, $10^{1.5}$, 10^2, $10^{2.5}$, and 10^3. Note that the case $R = 1$ corresponds to the original cross sections calculated in § 2.3. Figure 9 shows the results for the same lens parameters as in Figure 3, except that here only

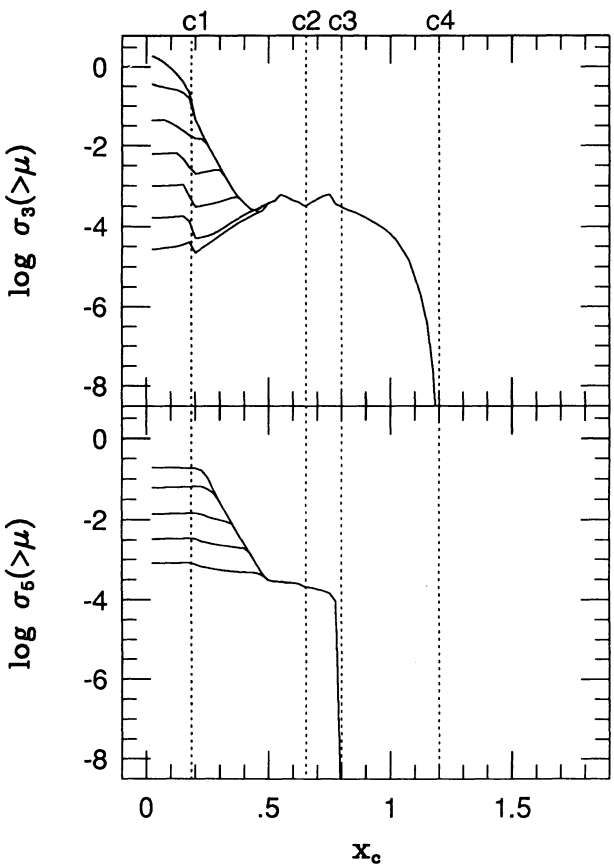

FIG. 9.—Cross sections for lensing by an $\epsilon = 0.2$ lens with brightest-to-dimmest image magnification ratio of $10^{1.5}$ or greater. The vertical lines indicate the critical points in the core radius defined in § 2.2. Comparing with Fig. 3, it can be seen that the cross sections are the same for very small core radii ($x_c \lesssim c_1$), but for larger cores the cross sections fall off more rapidly than in Fig. 3.

source positions which have $R > 10^{1.5}$ are included. At small core radii, the curves in Figure 9 are very similar to those in Figure 3, which shows that these lenses almost always produce a very weak odd image (weaker than $10^{-1.5}$ of the strongest image). However, Figures 3 and 9 deviate significantly as the core radius increases, implying that images of very disparate brightnesses become progressively less likely at large core radii.

To obtain quantitative results, we need to estimate the limiting magnitudes of the missing images in the observed examples of lensing. From the observational limits of the lensed quasars, we estimate that the central images must be at least 10–100 times fainter than the observed bright images in order to have escaped detection. This corresonds to $R > 10$–100, and so we present results corrsponding to $R = 10^{1.5}$.

For this choice of R and for a core radius of 200 pc, we find that 80% of triply imaged systems will have an unobserved central image. This is roughly consistent with the observations where only one lens, viz., Q2016+112, shows any sign of the central image, and even in this case the image may equally well be interpreted as a pair of merging outer images (Narasimha et al. 1987). For other core radii the results are as follows: if the core radius is 100 pc, nearly 95% of triples will have a missing central image at the $10^{-1.5}$ level, and for 300, 400, and 500 pc it is 60%, 35%, and 15%, respectively. We conclude from this that the core radii of lenses have to be less than about 200 pc. This limit is consistent with measured core radii of a few nearby galaxies (Lauer 1985), but the present result is of course more general, since it applies to the entire population of galaxies at all redshifts.

Interestingly, it is considerably easier to hide the central image in quadruples than in doubles. Our results show that nearly 100% of five-image systems will have $R > 10^{1.5}$ for a core radius of 200 pc, and as many as 75% will satisfy this limit even for a core radius of 500 pc. Therefore, the absence of the central image in the observed quadruples provides less of a constraint. Incidentally, if $\xi_c^* > 1000$ pc (which we consider in the following section), then the vast majority of both doubles and quadruples would have central images significantly brighter than the $R = 10^{1.5}$ limit considered here.

5.4. *Gravitational Lensing of BL Lacertae Objects*

In this section we use our model to analyze the interesting suggestion of Ostriker & Vietri (1985, 1990, hereafter collectively OV) that BL Lacertae objects may be lensed quasars.

BL Lac objects are polarized, highly variable extragalactic sources which are generally believed to be active galactic nuclei with relativistic beams that are nearly aligned along the line of sight. OV noted that there is a statistical overpopulation of BL Lac objects at low redshifts, and proposed that these objects may actually be distinct optically violently variable quasars and that the measured redshifts usually associated with the BL Lac objects really correspond to foreground galaxies which act as gravitational lenses and cause an apparent brightening of the quasars. They explained the lack of QSO emission lines by proposing that microlensing by stars or black holes amplifies the continuum emission relative to the lines. By analyzing a very simple lens model consisting of a constant-density disk of matter, OV found that the magnification of a distant quasar reaches a maximum for lens positions corresponding to two redshifts, one near the observer and one near the source. They proposed that the apparent overdensity of BL Lac objects at low redshift is the result of the nearer of the two peaks, coupled with magnification bias. The recent discovery by Stickel, Fried, & Kuhr (1988a, b, 1989) that the galaxies apparently associated with three BL Lac objects are actually foreground objects appears to support OV's proposal.

We have used our calculated cross sections and simulations of number counts to examine this proposal. There are two details in which our models are superior to the constant-density disk employed by OV. First, our lenses have a more realistic radial structure, with a finite core radius and an isothermal profile outside the core. Second, our models include ellipticity. In order to match the central density of our lenses to the constant mass density of 2 g cm^{-3} used by OV, we adopt a linear core radius of 1200 pc.

Figure 10 shows the results for a circularly symmetric lens with the above core radius. Plotted as a function of redshift are the probabilities of producing either a brightened single image or three images. The probabilities are calculated by converting the x_c dependence of the cross sections directly to z using equation (2.4) and by including the cosmological weighting function $w'(z_d, z_s)$. The distribution for a single highly magnified image shows peaks at two lens redshifts, one close to the observer and one close to the source, exactly as in the OV model. The shapes of the peaks are different in detail, but the general characteristics are quite similar. However, a comparison with the distribution of three-image cross sections reveals a problem. At all reasonable magnifications ($\mu \gtrsim 10$), the cross section for producing three images is significantly higher than that for producing a single bright image (Kochanek 1991b). Furthermore, three-image configurations are present for a

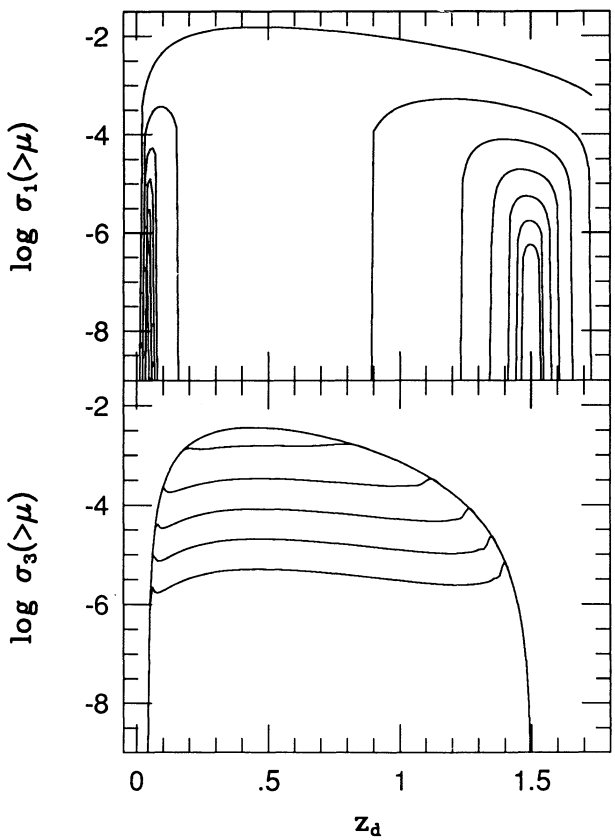

FIG. 10.—Probability of lensing by a circularly symmetric lens with $\xi_c^* = 1200$ pc as a function of redshift. The cosmological weighting function $w'(z_d, z_s)$ has been included. The peaks in the single-image cross sections seen by Ostriker & Vietri (1990) at high magnifications are clearly visible.

much wider range of redshifts. For both reasons, we would expect that for every example of a high-redshift optically violently variable quasar that is lensed to produce a BL Lac object, there should be a large number of similar quasars that are multiply imaged. There is no evidence for this in the observations.

Figure 11 shows next the effect of including ellipticity in the lens model. In this case, we have displayed the probabilities of producing one, three, and five images. The situation is now even less favorable. The two peaks seen in the single-image curves in Figure 10 have virtually disappeared. Instead we now find that bright single images are possible over most of the redshift range between the observer and the source. This is

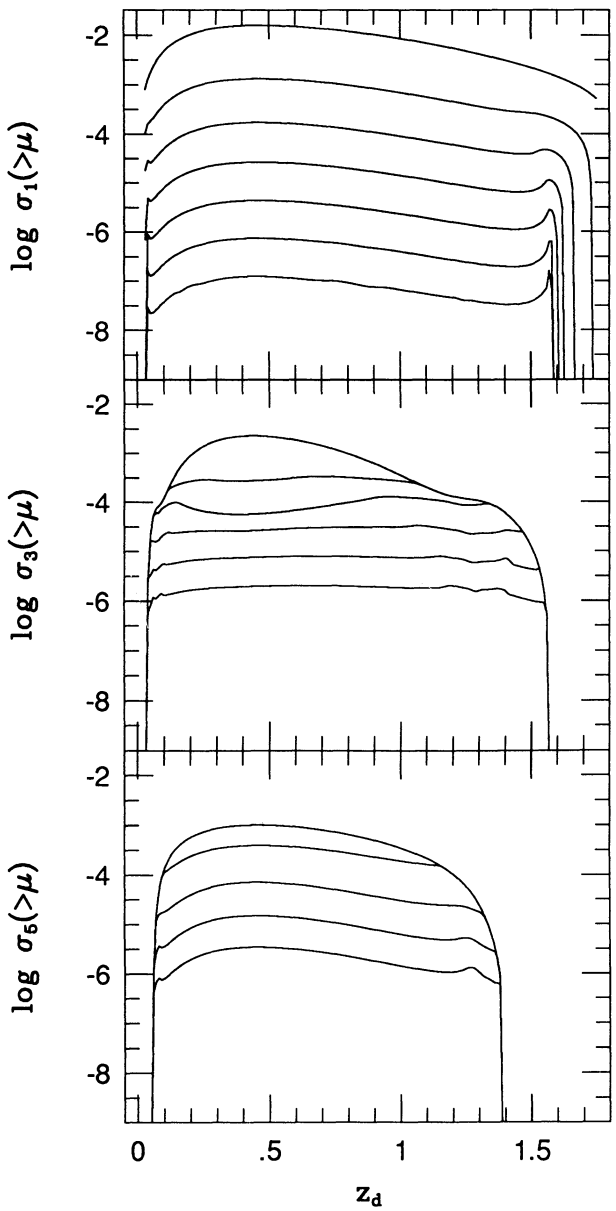

FIG. 11.—Probability of lensing by an elliptical lens with $\epsilon = 0.2$ and $\xi_c^* = 1200$ pc as a function of redshift. The weighting function $w'(z_d, z_s)$ has been included. Notice that the peaks in the single-image cross sections that were very noticeable in Fig. 10 have nearly disappeared with the addition of ellipticity.

because an elliptical lens can have exposed cusps which can produce highly brightened single images for a wide range of parameters, particularly when the core radius is as large as in the present example. Once again, the cross sections for three and five images are larger than those for a single image, a problem for the OV model.

Based on these results, it would appear that the OV proposal for BL Lac objects is ruled out. We must caution, however, that we cannot draw such a conclusion yet from our results. Our analysis is limited to consideration of the smooth matter in the lens, whereas a major ingredient of the OV model is the effect of microlensing, which might make a considerable difference. For instance, in the single-image configurations corresponding to the two favorable redshifts considered by OV, the image tends to be located in the core of the lens. On the other hand, in multiple imaging, the images invariably fall outside the core. Also, the bright single images at intermediate redshifts obtained with an elliptical lens again fall outside the core because they are due to exposed cusps. If microlenses had a much higher number density in the core of the lens than elsewhere, and if microlensing were to introduce an extremely large magnification bias, then one could imagine, in principle, that the configurations with single images in the core might be considerably overrepresented in the observations. One would then have a situation similar to that considered by OV.

Regardless of the validity of the particular model proposed by OV, we do have to deal with the observational fact that three BL Lac objects appear to have low-redshift galaxies in front of them (Stickel et al. 1988a, b, 1989). Narayan & Schneider (1990) analyzed two of these objects and concluded that the respective galaxies must have core radii greater than $\sim$1000–1500 pc in order not to produce multiple images of the quasars. This limit is consistent with the core size required in the OV hypothesis but is much larger than the upper limit to the core radius derived in the previous section. If the relevant observations are reliable, then these conflicting results may imply that they are two populations of galaxies with very different core radii.

6. CONCLUSION

In this paper we analyze in detail gravitational lensing cross sections corresponding to an elliptical lens. We model the lens by means of a simple potential with three parameters: the velocity dispersion σ, the ellipticity ϵ, and the linear core radius ξ_c. We use galaxy data to derive the distributions of σ and ϵ, and propose a simple scaling (eq. [3.2]) whereby the core radii of different lenses are written in terms of a single parameter, viz., the core radius, ξ_c^*, of an L_* galaxy. Since very little is known about the core radii of galaxies, we treat ξ_c^* as a free parameter and calculate our results for a range of values. With this model we simulate gravitational lensing of quasars, using a quasar luminosity function which extends out to a redshift of $z = 5$.

Our overall conclusion is that we can reproduce the main features of the observations quite well. We predict on the basis of our models that one in a few hundred quasars brighter than 17 mag should be multiply imaged in agreement with the observed lensing frequency, which is approximately 1 in 100 at this magnitude limit. Also, we predict that among these bright lenses there should be roughly equal numbers of doubles and quadruples, again in agreement with the observations. These results confirm the conclusions of earlier work by Kochanek (1991b) and Fukugita & Turner (1991), but the present work is

an improvement in some ways: whereas Fukugita & Turner considered only circularly symmetric lenses, we have included the effects of ellipticity (as did Kochanek 1991b). Further, the galaxy distributions we employ are based on the well-characterized sample of galaxies obtained with the CfA redshift survey (Huchra et al. 1983) and are therefore more complete. Also, our quasar luminosity function uses more up-to-date observations.

The main new feature of our work is that we have done our calculations for a range of lens core radii. We are therefore able to compare the model predictions with the observations and set limits on the core radius of galaxy lenses. The most sensitive test is provided by the missing image in the observed examples of multiple imaging.

As is well known, the multiply imaged quasars with two and four images should really have three and five images, respectively, with the extra image being located near the center of the lensing galaxy. The central images are thought to be missing because they are strongly demagnified (Narayan et al. 1984). Since the magnification of this image is determined primarily by the core radius of the lens, the observed limits on the brightnesses of the missing images can be translated to a bound on the core radius parameter ξ_c^*. Using this argument, we conclude that $\xi_c^* \lesssim 200$ pc.

There are other indications as well for such small core radii. The overall probability of lensing predicted by the model, and the relative numbers of doubles and quadruples, are both in best agreement with the observations when we use core radii less than a few hundred parsecs. To our knowledge, the distribution of core radii of distant galaxies is essentially unknown, and even for nearby galaxies there are very few direct measurements (cf. Lauer 1985).

The issue of core radii is unfortunately complicated by the discovery of (apparently) foreground galaxies in front of a few BL Lac objects (Stickel et al. 1988a, b, 1989). These particular galaxies must have core radii greater than 1000 pc in order not to produce multiple images of the respective background BL Lac objects (Narayan & Schneider 1990). This lower limit is in conflict with the upper limit we derived above. One way out of this disagreement is to postulate that the galaxies involved are not in the foreground but are actually associated with the BL Lac objects. This would make the galaxies unusually bright. Alternatively, we might consider the possibility that galaxies come in two types, each with different core radii. In this scenario, galaxies with small cores (mostly ellipticals?) produce multiply imaged quasars, while galaxies with large cores (spirals?) cause something like the BL Lac phenomenon, where a background quasar is brightened, but not multiply imaged, by lensing. This idea, coupled with magnification bias associated with microlensing, is the model proposed by OV for BL Lac objects. However, as we showed in § 5.4, there are more serious, though not necessarily fatal, problems with this picture.

Yet another complication to consider is that the centers of galaxies may contain compact mass concentrations such as supermassive black holes or dense star clusters. If there is enough mass in such structures, then the missing image could be "swallowed" by the mass concentration (Subramanian, Chitre, & Narasimha 1985; Narasimha et al. 1987) despite the rest of the galaxy having a large core radius. In such cases we can think of the lens as having effectively two cores: a very compact core which eliminates the central image, and another, potentially much larger, core associated with the smooth mass. The structure of the latter may not be probed very well by lensing except when the first component is weak or missing altogether.

Finally, using our models, we have quantified the degree to which magnification bias affects the sample of lensed quasars. We find that the bias is extremely strong at bright magnitudes, particularly for quadruples. Consequently, the largest frequency of lensing (by far) occurs at magnitudes brighter than about 16 or 17 mag. The northern sky has already been surveyed fairly well at these magnitudes. It seems to us that the easiest way to enlarge the sample of multiply imaged quasars is to survey the entire southern sky down to similar magnitudes. Pushing searches to fainter magnitudes will also, of course, produce more examples of lensing, but the magnification bias drops rapidly. Consequently, such searches will yield relatively fewer examples of lensing per source studied. These statements are true only for optical searches. The situation with radio surveys, which will depend on the luminosity function of high-redshift radio sources has not been analyzed. Also, radio sources are typically extended and resolved, which complicates the analysis (Kochanek & Lawrence 1990).

We thank John Huchra for his comments and for providing galaxy data from the CfA Redshift Survey, and Christopher Kochanek for comments. This work was supported in part by a grant (AST-9109525) from the National Science Foundation. R. N. was also supported by a Presidential Young Investigator award.

REFERENCES

Blandford, R. D., & Kochanek, C. S. 1987a, in Dark Matter in the Universe, ed. J. Bahcall, T. Piran, & S. Weinberg (Berlin: Springer-Verlag), 133
———. 1987b, ApJ, 321, 658
Blandford, R. D., Kochanek, C. S., Kovner, I., & Narayan, R. 1989, Science, 245, 824
Blandford, R. D., & Narayan, R. 1992, ARA&A, 30, 311
Boyle, B. J., Shanks, T., & Peterson, B. A. 1988, MNRAS, 235, 935
Dyer, C. C. 1984, ApJ, 287, 26
Falco, E. E., Gorenstein, M. V., & Shapiro, I. I. 1991, ApJ, 372, 364
Fort, B. 1992, in Gravitational Lenses, ed. R. Kayser, T. Schramm, & L. Nieser (Berlin: Springer-Verlag), 267
Fukugita, M., & Turner, E. L. 1991, MNRAS, 253, 99
Gott, J. R., & Gunn, J. E. 1974, ApJ, 190, L105
Hacyan, S. 1982, Astrophys. Lett, 22, 97
Heflin, M. B., Gorenstein, M. V., Lawrence, C. R., & Burke, B. F. 1991, ApJ, 378, 519
Hewitt, A., & Burbidge, G. 1987, ApJS, 63, 1
Hinshaw, G., & Krauss, L. M. 1987, ApJ, 320, 468
Huchra, J., Davis, M., Latham, D., & Tonry, J. 1983, ApJS, 52, 89
Irwin, M., McMahon, R. G., & Hazard, C. 1991, in Space Distribution of Quasars, ed. D. Crampton (ASP Conf. Ser., Vol. 21; San Francisco: ASP), 117
Kayser, R., Surdej, J., Condon, J. J., Kellermann, K. I., Magain, P., Remy, M., & Smette, A. 1990, ApJ, 364, 15
Kochanek, C. S. 1991a, ApJ, 373, 354
———. 1991b, ApJ, 379, 517
———. 1991c, ApJ, 382, 58
Kochanek, C. S., & Blandford, R. D. 1987, ApJ, 321, 676
Kochanek, C. S., & Lawrence, C. R. 1990, AJ, 99, 1700
Lauer, T. R. 1985, ApJ, 292, 104
Lawrence, C. R., Schneider, D. P., Schmidt, M., Bennett, C. L., Hewitt, J. N., Burke, B. F., Turner, E. L., & Gunn, J. E. 1984, Science, 223, 46
Mao, S. 1991, ApJ, 380, 9
Narasimha, D., Subramanian, K., & Chitre, S. M. 1982, MNRAS, 200, 941
———. 1987, ApJ, 315, 434
Narayan, R. 1991, ApJ, 378, L5

Narayan, R., Blandford, R. D., & Nityanada, R. 1984, Nature, 310, 112
Narayan, R., & Grossman, S. 1989, in Gravitational Lenses, ed. J. M. Moran, J. N. Hewitt, & K.-Y. Lo (Berlin: Springer-Verlag), 31
Narayan, R., & Schneider, P. 1990, MNRAS, 243, 192
Narayan, R., & White, S. D. M. 1988, MNRAS, 231, 97P
Ostriker, J. P., & Vietri, M. 1985, Nature, 318, 446
———. 1990, Nature, 344, 45
Schmidt, M., Schneider, D. P., & Gunn, J. E. 1991, in Space Distribution of Quasars, ed. D. Crampton (ASP Conf. Ser., Vol. 21; San Francisco: ASP), 109
Schneider, P., Ehlers, J., & Falco, E. E. 1992, Gravitational Lenses (Berlin: Springer-Verlag)
Stickel, M., Fried, J. W., & Kuhr, H. 1988a, A&A, 198, L13
———. 1988b, A&A, 206, L30
Stickel, M., Fried, J. W., & Kuhr, H. 1989, A&A, 224, L27
Subramanian, K., Chitre, S. M., & Narasimha, D. 1985, ApJ, 289, 37
Surdej, J., Magain, P., Swings, J.-P., Borgeest, U., Courvoisier, T. J.-L., Kayser, R., Kellermann, K. I., Kuhr, H., & Refsdal, S. 1988, A&A, 198, 49
Surdej, J. 1990, in Gravitational Lensing, ed. Y., Mellier, B. Fort, & G. Soucail (Berlin: Springer-Verlag), 57
Turner, E. L. 1980, ApJ, 242, L135
Turner, E. L., Ostriker, J. P., & Gott, J. R. 1984, ApJ, 284, 1
Tyson, J. A. 1983, ApJ, 272, L41
Walsh, D., Carswell, R. F., & Weymann, R. J. 1979, Nature, 279, 381
Warren, S. J., Hewitt, P. C. & Osmer, P. S. 1991, in Space Distribution of Quasars, ed. D. Crampton (ASP Conf. Ser., Vol. 21; San Francisco, ASP), 139
Wu, X. P. 1989, A&A, 214, 43